


Novel approach to light-cluster production in heavy-ion collisionsHui-Gan Cheng and Zhao-Qing Feng ^{*}*School of Physics and Optoelectronics, South China University of Technology, Guangzhou 510640, China*

(Received 8 November 2023; accepted 25 January 2024; published 15 February 2024)

The issue of cluster production in heavy-ion collisions is addressed in a new manner, by implementing cluster correlation into the quantum molecular dynamics (QMD) transport model. We demonstrate for the first time, the good potentialities of this popular transport approach in the unified description of light-cluster production including the deuteron, the triton, ^3He , and the α cluster in heavy-ion collisions at intermediate energies. Both the INDRA and FOPI experimental data of the yields of light clusters and the charge distributions of heavier fragments are reasonably reproduced in a unified manner. The effects of both the cluster binding energies and the Pauli repulsion are also shown to play crucial roles in the production of clusters.

DOI: [10.1103/PhysRevC.109.L021602](https://doi.org/10.1103/PhysRevC.109.L021602)

The emergence of clusters is of nontrivial interest, sometimes central importance, in the study of nuclear physics [1–8]. In the particular study of heavy-ion collisions (HICs) at incident energies of tens of MeV to hundreds of MeV, for instance, the yields of deuterons, tritons, ^3He , and α particles are comparable with or even greater than the yield of protons [9]. The huge effects of clusters on the equation of state (EoS) of nuclear matter have already been revealed in the low-density regime [10]. Thus, the crucial role played by clusters in the dynamical evolution of the reaction system is also supposed to have an impact [9,11] on the final-state observables which furnish probes to the nuclear EoS in the high-density regime [12–14]. Therefore, cluster is an unavoidable aspect which deserves explicit treatments in transport approaches for HICs. In astrophysical studies, just like the pasta phase [15–17], the rich cluster contents in dilute and warm nuclear matter [18–20] also have significant relevance in the core-collapse of supernovae and the properties and evolution of compact stars [21,22].

In HICs at higher energies, for example, several GeV/nucleon at FAIR [23–25], RHIC-STAR [26–28], NICA [29], and HIAF [30] in the future, hypernuclei are abundantly created. They furnish interesting laboratories to study the two- or three-body hyperon interactions which lie at the heart of the understanding of the structure of compact stars [31,32]. The dynamics of hypernucleus production in the midrapidity regions may be reasonably reproduced simply by baryon coalescence in central HICs [28]. However, light clusters are also copiously produced in the spectator rapidity regions and in semicentral or peripheral collisions [33–37]. This is reminiscent of fireball-spectator fragmentation [37–39] where coalescence is not applicable and of the interesting formation mechanism of hypernuclei through the capture of hyperons by spectator clusters [40]. It is, thus, a prerequisite to properly account for the issue

of clusters in the nonfireball regions [37] which break up at intermediate energies. This may also open the perspective to study the nuclear liquid-gas phase transition with hyperons and the production of hypernuclei of extreme isospin.

In the past and in very recent years, explicit treatment of clusters has well been incorporated into transport models like the anti-symmetrized molecular dynamics model (AMD) [41,42] or the Boltzmann-Uehling-Uhlenbeck model [43–50], which are capable of describing the production of clusters even up to α [41–43]. They promise excellent theoretical tools in the study of the various effects of clusters in HICs, for example, the extraction of the high-density EoS [11], fragment formation [51,52], nucleosynthesis in ultrarelativistic HICs [48,50], and so on. It is rather intriguing, however, to also see similar attempts [53] based on another popular class of model, the quantum molecular dynamics (QMD) transport model [54], which accounts for the branching of the system into different final-state fragment partitions and is readily applicable to high energies, furnishing excellent opportunities to investigate the abovementioned cases where cluster and strangeness join to play an interesting role.

In this Letter, we address the issue of clusters in heavy-ion collisions from a new perspective, by implementing in the QMD model the kinetic production of clusters including deuterons, tritons, ^3He , and the α particle for the first time, leading to a good description of the production of both light clusters and heavier fragments in a unified manner, as compared to the INDRA [55,56] and FOPI [57] data, furnishing a starting point to the abovementioned studies. The effects of both the cluster binding energies and the Pauli repulsion on clusters [58] have also been shown to play vital roles in the production of clusters.

In the treatment of cluster production, we follow the method proposed by Ono in AMD clusters, as documented in previous articles [41,42]. The basic idea is to include quantum transition to clustered states up to the production of α as possible final states of the scattering between two nucleons, N_1N_2 . Starting from the nonclustered NN

^{*}fengzqh@scut.edu.cn

scattering final state, repeated steps are taken by constructing the projection operator $\hat{P} = \sum_{ij} |P_i\rangle\langle N^{-1}|_{ij}\langle P_i|$ for the subspace of clustered states $|P_i\rangle$ at each step, to consider all scattering channels $C_1 + C_2 \rightarrow C_3 + C_4$ between nucleon-nucleon, nucleon-cluster, and cluster-cluster in a unified manner. The actual treatment, however, is much more complicated. Denote the state of the reaction system before NN scattering as $|O\rangle$, and denote the state after ordinary NN scattering without considering clusters and energy conservation as $|P\rangle$. We need to adjust the relative momentum between N_1 and N_2 in the nonclustered state $|P\rangle$ to a new nonclustered state, $|Q\rangle$, from which the energy-conserving clustered final state can be constructed. If we assume the transition amplitude of the process to be $P(C_1 + C_2 \rightarrow C_3 + C_4)|T(\tilde{p}_{\text{rel}})|^2$, where $|T(\tilde{p}_{\text{rel}})|$ is the ordinary NN scattering transition amplitude evaluated at the average relative NN momentum \tilde{p}_{rel} of $|O\rangle$ and $|Q\rangle$, the differential cross section of the process can be cast as follows:

$$\frac{d\sigma}{d\Omega} = P(C_1 + C_2 \rightarrow C_3 + C_4) \times \frac{v_{\tilde{p}_{\text{rel}}}}{v} \frac{|[\partial e(k)/\partial k]_{k=\tilde{p}_{\text{rel}}}|}{|[\partial H(p_f)/\partial p_f]_{p_f=\tilde{p}_{\text{rel}}}|} \frac{p_{\text{rel}}^2}{\tilde{p}_{\text{rel}}^2} \left[\frac{d\sigma_{\text{NN}}}{d\Omega} \right]_{\tilde{p}_{\text{rel}}}. \quad (1)$$

Here v is the NN relative velocity in $|O\rangle$ and $v_{\tilde{p}_{\text{rel}}}$ is that under \tilde{p}_{rel} . p_{rel} is the relative momentum between $N_1 N_2$ in $|Q\rangle$. $e(k)$ is the kinetic energy of the two nucleons in free space and H is the total energy of the reaction system. Both $e(k)$ and $H(p_f)$ are functions of the relative momentum between $N_1 N_2$. The last factor in the expression is the ordinary free-space differential NN cross section evaluated at \tilde{p}_{rel} :

$$H = \sum_i \frac{\mathbf{p}_i^2}{2m} + \frac{\alpha}{2} \sum_{\substack{i,j \\ j \neq i}} \frac{\rho_{ij}}{\rho_0} + \frac{\beta}{1+\gamma} \sum_i \left(\sum_{\substack{j \\ j \neq i}} \frac{\rho_{ij}}{\rho_0} \right)^\gamma + \frac{C_{\text{sym}}}{2} \sum_{\substack{i,j \\ j \neq i}} t_{z_i} t_{z_j} \frac{\rho_{ij}}{\rho_0} + \frac{g_{\text{sur}}}{2} \sum_{\substack{i,j \\ j \neq i}} \left[\frac{3}{2L} - \left(\frac{\mathbf{r}_i - \mathbf{r}_j}{2L} \right)^2 \right] \frac{\rho_{ij}}{\rho_0} + \sum_i^{N_c} E_{z.p.}^i + \sum_i^{N_d} V_{\text{corr}} e^{-r_i^2/4L} + V_{\text{Coul}}. \quad (2)$$

For the mean-field evolution of the reaction system, we employ the usual standard form of the Hamiltonian average in the Lanzhou quantum molecular dynamics (LQMD) model [59], but with slight modifications as shown in the above equation. We turn off the surface interaction term between any two nucleons among each cluster, as indicated by the extra prime added to the summation in the g_{sur} term, so that all the nucleons within a cluster move as a single object under the surface potential. The last but two term is a summation over the zero-point potential energy contributed by each cluster. This represents the internal quantum kinetic energy of nucleons within a cluster, and we adopted the form defined in Ref. [60]. But for the width and the smearing parameters defined in Ref. [60], we take $a = 0$ fm and $b = 2.25 \times 2.25$ fm² to guarantee that no local energy-minima are encountered in the dissolution of clusters, as is described later. Finally, in the last but one term, the binding energy of the deuteron is corrected

by artificially adding a term, where $V_{\text{corr}} = 1$ MeV, r_i is the relative distance between the wave-packet centers of the two nucleons, and $L = 1.75$ fm² is the wave-packet width parameter tuned here for LQMD to reasonably reproduce the binding energy of all light clusters. With the above prescription, the binding energy per nucleon of the deuteron is then 1.15 MeV, close to the experimental value. Other parameters in the above equation are $\alpha = -226.5$ MeV, $\beta = 173.7$ MeV, $\gamma = 1.309$, $C_{\text{sym}} = 38$ MeV, $g_{\text{sur}} = 23$ MeV fm², and $\rho_0 = 0.16$ fm⁻³.

In the AMD clusters, cluster correlation is only allowed where the nucleon density is above $\rho_{\text{cut}} = 0.125$ fm⁻³ [61]. In AMD or extended quantum molecular dynamics (EQMD) [60], a very large portion of the nucleon kinetic energy appears as the quantum zero-point motion of the Gaussian wave function. For this reason, the centroids of the nucleons' wave packets move faster in QMD than in AMD or EQMD so that it is more difficult to form clusters due to lower overlap between the wave packets. Meanwhile the density distribution of the system fluctuates more violently with faster moving nucleons. Thus, with the same form of in-medium NN cross section employed [42], to ensure that the same amount of cluster correlation is seen in both AMD clusters and QMD, we are forced to adopt a higher density cut $\rho_{\text{cut}} = 0.170$ fm⁻³ in our case.

The fermionic nature of the nucleon is a fundamental aspect in the formation and evolution of clusters in HICs. That the nucleon is a fermion is important in two aspects, mainly due to the exchange terms in the Hamiltonian average of a fermionic system. The exchange part of the kinetic energy term leads to the Pauli repulsion between fermions which can be mimicked by introducing a Pauli potential [62–64] or with the method of phase-space constraint [65] in QMD. The exchange part in the interaction term accounts for the change of the strength of binding among the nucleons within a cluster moving in nuclear media (Mott effect). At present, we only included the Pauli repulsion effect, while the Mott effect is left for future improvements.

The method of phase-space constraint was proposed by Papa *et al.* [65] in their constrained molecular dynamics model to render the phase-space occupation number f_i 's below 1 around every nucleon i in the course of mean-field evolution by a series of NN scatterings, but this is not viable when it comes to the case with clusters, since the evolution of nucleons is not continuous in momentum space with this method, which would destroy all formed cluster structures. For a remedy to this deficiency, a more delicate treatment is in order. We define a phase-space compactness function U_i in the form of a Pauli potential defined in Ref. [60], to measure the compactness of nucleons in each phase-space region P_i defined in the following, and lower U_i continuously by the technique of frictional cooling [66] under all conserved quantities of the reaction system, until the f_i 's are approximately all below a given bound $f_{\text{bound},i}$. For each spin-isospin, the P_i 's are identified by an elaborate minimum spanning tree (MST) procedure which divides the system into different phase-space regions by requiring that $k_{ij} \leq 6a\sqrt{L}$ is fulfilled between each pair of nucleons i and j within an identified phase-space region, where $k_{ij}^2 = [a(\mathbf{r}_i - \mathbf{r}_j)]^2 + [(\mathbf{p}_i - \mathbf{p}_j)/2a\hbar]^2$, with $a = 0.4$ fm⁻¹. For each nucleon i , define a quantity M_i , which we

may call “marginality,” measuring the closeness of i to the boundary of the nucleon distribution in space. M_i is the number of nucleons within a sphere of radius $3\sqrt{L}$ and centered at i . Then the bound on the phase-space occupation of each nucleon i is defined as a hyperbolic tangential function,

$$f_{\text{boun},i} = f_{\text{boun},l} + \frac{f_{\text{boun},u} - f_{\text{boun},l}}{2} \left(\tanh \frac{M_i - \frac{M_u + M_l}{2}}{\frac{M_u - M_l}{4}} + 1 \right), \quad (3)$$

where the upper and the lower values of the bound are $f_{\text{boun},u} = 0.95$ and $f_{\text{boun},l} = 0.65$, and the corresponding marginalities M_i are $M_u = 17$ and $M_l = 8$. In this way, the process of phase-space constraint acts like a Pauli potential and the formation of clusters in dilute regions at the disintegration of the system can thus be favored by imposing a tighter $f_{\text{boun},i}$ which has the tightest value, $f_{\text{boun},l} = 0.65$, in the most dilute areas.

For the dissolution of clusters in mean-field evolution, at the end of each time step of mean-field evolution, an MST procedure is applied among the nucleons within each existing cluster, in which an MST criterion $k_{ij} \leq 1.75$ is satisfied between any two nucleons in an MST fragment. If a cluster is identified as consisting of more than one MST fragment, the mother cluster is destroyed and the daughter clusters are registered. For the formation of bigger clusters, an MST procedure is applied to the entire system with $r_0 = 3.5$ fm and $p_0 = 200$ MeV/c. If an MST fragment ($2 \leq A \leq 4$) contains, as its constituents, smaller existing clusters, all the smaller clusters are destroyed and the MST fragment is registered as a new existing cluster. In all cases, the conservation of energy is treated via frictional cooling.

In Fig. 1, we present the numbers of nucleons contained in the final-state deuterons, tritons, ${}^3\text{He}$, and α emitted in central HICs with different reaction systems at Fermi energies. Triangles stand for the results of the model, and solid circles stand for those of experiments. For the last two reaction systems on the right-hand side, the experimental data are displayed. For ${}^{129}\text{Xe} + {}^{118}\text{Sn}$ at 50A MeV, the INDRA data [55] are plotted, and for ${}^{197}\text{Au} + {}^{197}\text{Au}$ at 90A MeV, the FOPI data are plotted [57]. Since in the FOPI data, the multiplicity of α and ${}^3\text{He}$ are not explicitly given for ${}^{197}\text{Au} + {}^{197}\text{Au}$ at 90A MeV, we substitute the α multiplicity of ${}^{197}\text{Au} + {}^{197}\text{Au}$ at 120A MeV, in that the experimental α yield is constant within error bars around 120A MeV. Hot fragments are all deexcited at 600 fm/c through the GEMINI code. For all the reaction systems shown here, the yield of α prevails, and for the reaction systems for which the experimental results are available, the results of our model agree with the data reasonably. Upon examining the figure more carefully, it can also be pointed out that the isospin asymmetries of the reaction systems are also correctly reflected on the relative yields of tritons and ${}^3\text{He}$. For ${}^{16}\text{O} + {}^{16}\text{O}$ and ${}^{40}\text{Ca} + {}^{40}\text{Ca}$, which are isospin symmetric, the yield ratio of triton/ ${}^3\text{He}$ is almost 1, whereas in ${}^{129}\text{Xe} + {}^{118}\text{Sn}$ and ${}^{197}\text{Au} + {}^{197}\text{Au}$, which are neutron rich, this ratio is greater than 1. When the phase-space constraint is not applied, as indicated by the black short-dashed line for ${}^{129}\text{Xe} + {}^{118}\text{Sn}$, the yield of α is almost the same as that of tritons + ${}^3\text{He}$, and lower than that of deuterons. When this method is turned

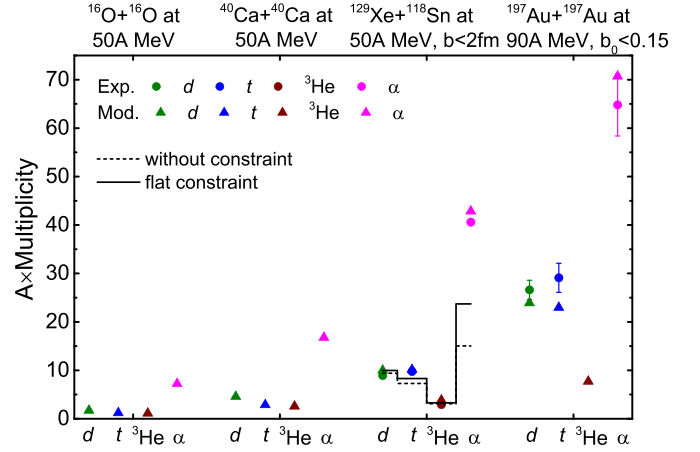


FIG. 1. The numbers of nucleons of each type of cluster, including the deuterons (olive), tritons (blue), ${}^3\text{He}$ (wine), and α particles (magenta), are plotted for the results of the model (solid triangles) and that of experiments (solid circles), with the INDRA data [55] for ${}^{129}\text{Xe} + {}^{118}\text{Sn}$ at 50A MeV and the FOPI data [57] for ${}^{197}\text{Au} + {}^{197}\text{Au}$ at 90A MeV, respectively. The data of α in the latter reaction system are taken from that of ${}^{197}\text{Au} + {}^{197}\text{Au}$ at 120A MeV, as explained in the text. The results without phase-space constraint (short-dashed line) and with “flat” phase-space constraint (solid line) are also plotted for ${}^{129}\text{Xe} + {}^{118}\text{Sn}$ at 50A MeV.

on but with the same $f_{\text{boun},i}$, that is, $f_{\text{boun},i} = 0.95$ for all nucleons, as indicated by the black solid line denoted as “flat constraint,” the yield of α particles almost doubles. And when we apply a stronger constraint to dilute regions, as described in the context earlier, the yield of α doubles again to match the experimental data. This can be attributed to both the global improvement of phase-space distribution of nucleons across the entire system and to a complex of factors brought by the stronger phase-space constraint in dilute regions. These mainly include the aggregation of smaller clusters and nucleons into bigger clusters, the reduced Pauli-blocking in forming clusters in scattering, the increased outward Pauli repulsion of the boundary regions upon α particles [58], and finally, the interplay among all these effects. For this reaction system, the time evolutions of all gas-phase clusters are also plotted in Fig. 2. We observe that above 120 fm/c, the multiplicities of all clusters already reach approximate constant values; therefore, concerning the production of clusters, the time cut to switch from the dynamical stage to the stage of statistical decay is not so important in our case. In Fig. 3, we show the charge distributions of fragments reproduced by our model in comparison with the experimental data, for central HICs with typical reaction systems. Roughly speaking, our model gives a reasonable reproduction of the experimental charge spectra for $Z \geq 2$. At higher energies, our model seems to underestimate the data for fragments of large charge number, as also seen in the QMD results in Ref. [56]. This is due to the scheme of centrality selection we adopted here and the fact that the results presented here are raw and unfiltered [56]. For ${}^{129}\text{Xe} + {}^{118}\text{Sn}$ at 50A MeV, the yields of intermediate mass fragments (IMF), which have more than one nucleon occupying a spin-isospin state, are underestimated due to a stronger

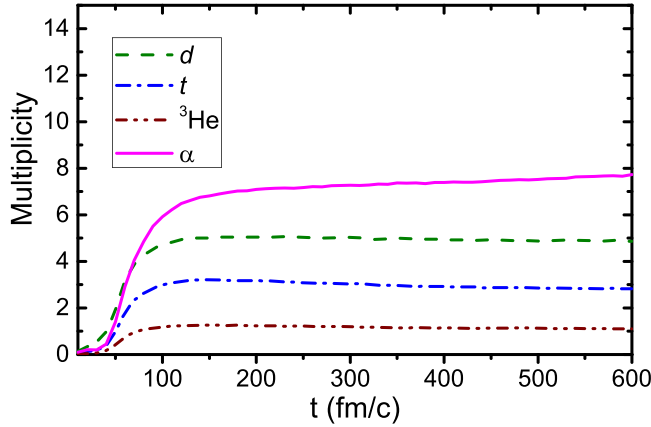


FIG. 2. The multiplicities of gas-phase clusters, including the deuterons (dashed line), the tritons (dot-dashed line), ${}^3\text{He}$ (dot-dot-dashed line) and the α particles (solid line), are plotted as functions of the evolution time of the reaction system ${}^{129}\text{Xe} + {}^{118}\text{Sn}$ at 50A MeV. Here the time starts at 10 fm/c when the two nuclei already overlap.

phase-space constraint on the dilute regions, the breeding place not only for clusters but also for IMF. In the meantime, the yields of heavy fragments are overestimated as a result of the lack of fragmentation due to the incompleteness of our description of the fermionic nature of nucleons. Another interesting result is that, in our model, the yield of fragments of $Z = 1$ are very much lower than the yield without cluster correlation [56] for ${}^{197}\text{Au} + {}^{197}\text{Au}$, which is a sign that the missing protons appear in gas-phase clusters. This is most apparent in ${}^{129}\text{Xe} + \text{CsI}$ at 150A MeV, where the yield of fragments of $Z = 1$ is close to the experimental value. In this particular reaction system, the production of very large fragments is negligible and the produced fireball ends up more

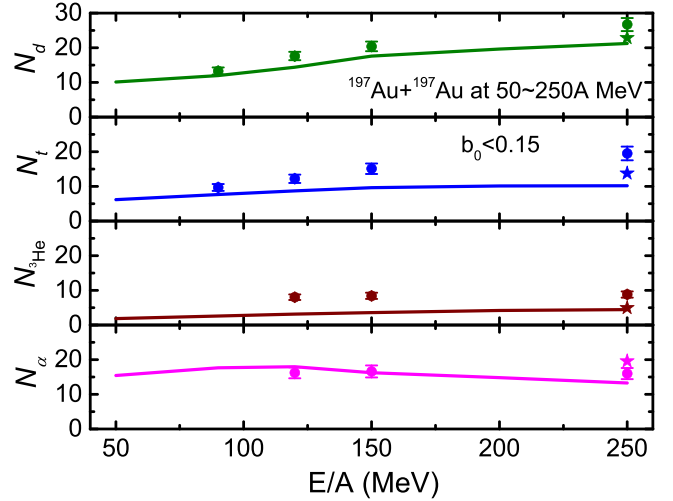


FIG. 4. The dependence of the yield of light clusters including the deuterons (olive), the tritons (blue), ${}^3\text{He}$ (wine), and the α particles (magenta) on the incident energy as plotted in solid lines for central ${}^{197}\text{Au} + {}^{197}\text{Au}$ collisions, in comparison with the FOPI data [57]. Here the early results of the AMD cluster [42] are also displayed as solid stars alongside for comparison.

gaslike, suppressing the spurious emission of nucleons from hot big fragments, which is due to the semiclassical nature of QMD. With the above observations, we can hitherto conclude that our model achieved, in a reasonable and unified description of both the yields of light clusters and heavier fragments, a first step towards a realistic description of hypercluster production in spectator fragmentation.

Finally, in Fig. 4, the dependence of the yields of light clusters on the incident energy is shown for central HICs with the reaction system ${}^{197}\text{Au} + {}^{197}\text{Au}$, in comparison with

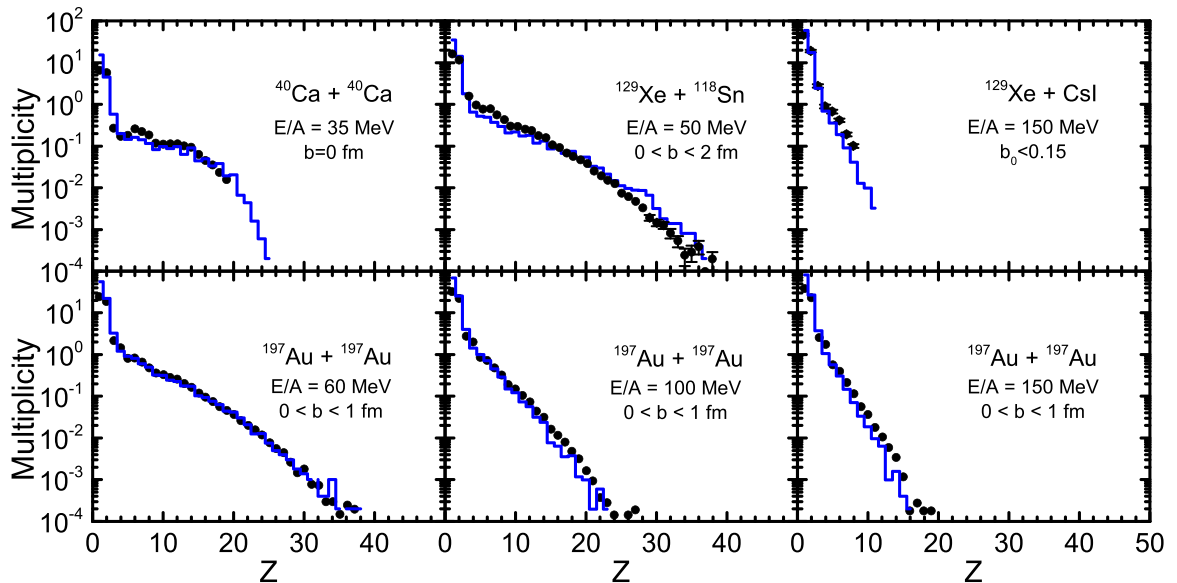


FIG. 3. The fragment charge distributions in central HICs are plotted as solid lines for various reaction systems in comparison with the experimental data (solid circles). The experimental results are respectively taken from Ref. [67] for ${}^{40}\text{Ca} + {}^{40}\text{Ca}$, the INDRA data [55] for ${}^{129}\text{Xe} + {}^{118}\text{Sn}$, the FOPI data [57] for ${}^{129}\text{Xe} + \text{CsI}$, and the INDRA data [56] for all the ${}^{197}\text{Au} + {}^{197}\text{Au}$ collisions in the lower panels. For the model, only the raw (unfiltered) results with centralities selected by an impact parameter cut are given.

available FOPI [57] data and the early results of AMD clusters [42]. First, we see that at the highest energy, 250A MeV, our result is very similar to that of AMD clusters, with the yields of deuterons, tritons, and ^3He underestimated, which is within our expectation since both models employ the same prescription in the treatment of cluster correlation. Finally, our model correctly describes the increasing trend of the yield of deuterons against the incident energy, and the experimental fact that the yield of α particles is almost a plateau over the shown incident energy range.

In conclusion, by implementing cluster correlation, a popular microscopic transport approach QMD is for the first time shown to be as well powerful in a unified description of the production of light clusters and heavier fragments in heavy-ion collisions, which may open the perspective for various future investigations. A method of continuous phase-space constraint based on the technique of frictional cooling is devised and acts like a Pauli potential to improve the phase-space distribution of nucleons, and facilitates the formation and emission of clusters through Pauli repulsion during the course of heavy-ion collisions. The binding energy of clusters is also considered and is important for the description of cluster production. A reasonable reproduction of both the

experimental light-cluster multiplicities including deuterons, tritons, ^3He , and α particles, and the experimental charge distributions of heavier fragments are achieved. The isospin asymmetries of the reaction systems are well reflected on the triton/ ^3He yield ratio, and as far as light-cluster production is concerned, the results are insensitive to the time cut to switch from QMD to the statistical afterburner. The trends of yields of different kinds of light clusters against incident energy are correctly reproduced. Imperfect it may be, but this work adds a valuable contribution to the development of the QMD model in terms of the study of light-cluster production in multifragmentation reactions at intermediate energies. This makes accessible the perspective for various promising future extensions, for example, hypercluster formation in spectator fragmentation reactions, in which the QMD model is endowed with special advantages.

The authors are indebted to Prof. A. Ono for helpful discussions on the details of the treatments and the relevant physics. This work was supported by the National Natural Science Foundation of China (Projects No. 12175072 and No. 12311540139) and the Talent Program of South China University of Technology (Project No. 20210115).

-
- [1] *Clusters in Nuclei*, edited by Christian Beck (Springer-Verlag, Berlin, Heidelberg, 2010), Vol. 1.
- [2] *Clusters in Nuclei*, edited by Christian Beck (Springer-Verlag, Berlin, Heidelberg 2012), Vol. 2.
- [3] *Clusters in Nuclei*, edited by Christian Beck (Springer International, Cham, Switzerland, 2014), Vol. 3.
- [4] H. Horiuchi, K. Ikeda, K. Kato, Recent developments in nuclear cluster physics, *Prog. Theor. Phys. Suppl.* **192**, 1 (2012).
- [5] J. P. Ebran, E. Khan, T. Niksic, D. Vretenar, How atomic nuclei cluster, *Nature (London)* **487**, 341 (2012).
- [6] Z. Z. Ren, B. Zhou, Alpha-clustering effects in heavy nuclei, *Front. Phys.* **13**, 132110 (2018).
- [7] D. M. Brink, History of cluster structure in nuclei, *J. Phys.: Conf. Ser.* **111**, 012001 (2008).
- [8] G. Röpke, Clusters in nuclear matter and Mott points, *Phys. Part. Nuclei* **46**, 772 (2015).
- [9] A. Ono, Dynamics of clusters and fragments in heavy-ion collisions, *Prog. Part. Nucl. Phys.* **105**, 139 (2019).
- [10] J. Natowitz, G. Röpke, S. Typel, D. Blaschke, A. Bonasera, K. Hagel, T. Klähn, S. Kowalski, L. Qin, S. Shlomo, R. Wada *et al.*, Symmetry energy of dilute warm nuclear matter, *Phys. Rev. Lett.* **104**, 202501 (2010).
- [11] N. Ikeno, A. Ono, Y. Nara, and A. Ohnishi, Probing neutron-proton dynamics by pions, *Phys. Rev. C* **93**, 044612 (2016); **97**, 069902(E) (2018).
- [12] B. A. Li, Probing the high density behavior of the nuclear symmetry energy with high energy heavy-ion collisions, *Phys. Rev. Lett.* **88**, 192701 (2002).
- [13] J. Estee *et al.* ($S\pi$ RIT Collaboration), Probing the symmetry energy with the spectral pion ratio, *Phys. Rev. Lett.* **126**, 162701 (2021).
- [14] P. Danielewicz, R. Lacey, and W. G. Lynch, Determination of the equation of state of dense matter, *Science* **298**, 1592 (2002).
- [15] M. E. Caplan and C. J. Horowitz, Colloquium: Astromaterial science and nuclear pasta, *Rev. Mod. Phys.* **89**, 041002 (2017).
- [16] C. J. Horowitz, D. K. Berry, C. M. Briggs, M. E. Caplan, A. Cumming, and A. S. Schneider, Disordered nuclear pasta, magnetic field decay, and crust cooling in neutron stars, *Phys. Rev. Lett.* **114**, 031102 (2015).
- [17] Z. D. Lin, M. E. Caplan, C. J. Horowitz, and C. Lunardini, Fast neutrino cooling of nuclear pasta in neutron stars: Molecular dynamics simulations, *Phys. Rev. C* **102**, 045801 (2020).
- [18] L. Qin, K. Hagel, R. Wada, J. B. Natowitz *et al.*, Laboratory tests of low density astrophysical nuclear equations of state, *Phys. Rev. Lett.* **108**, 172701 (2012).
- [19] K. Hagel, R. Wada, L. Qin, J. B. Natowitz *et al.*, Experimental determination of in-medium cluster binding energies and Mott points in nuclear matter, *Phys. Rev. Lett.* **108**, 062702 (2012).
- [20] H. Pais, R. Bougault, F. Gulminelli *et al.*, Low density in-medium effects on light clusters from heavy-ion data, *Phys. Rev. Lett.* **125**, 012701 (2020).
- [21] K. Sumiyoshi and G. Röpke, Appearance of light clusters in post-bounce evolution of core-collapse supernovae, *Phys. Rev. C* **77**, 055804 (2008).
- [22] M. Oertel, M. Hempel, T. Klähn, and S. Typel, Equations of state for supernovae and compact stars, *Rev. Mod. Phys.* **89**, 015007 (2017).
- [23] H. H. Gutbrod, I. Augustin, H. Eickhoff, K. D. Groß, W. F. Henning, D. Krämer, and G. Walter, *FAIR Baseline Technical Report* (GSI, Darmstadt, 2006).
- [24] J. Äystö *et al.*, Experimental program of the Super-FRS Collaboration at FAIR and developments of related instrumentation, *Nucl. Instrum. Methods Phys. Res. Sect. B* **376**, 111 (2016).

- [25] H. Geissel *et al.*, The Super-FRS project at GSI, *Nucl. Instrum. Methods Phys. Res. Sect. B* **204**, 71 (2003).
- [26] M. Abdallah *et al.* (STAR Collaboration), Measurements of ${}^3_{\Lambda}\text{H}$ and ${}^4_{\Lambda}\text{H}$ lifetimes and yields in Au + Au collisions in the high baryon density region, *Phys. Rev. Lett.* **128**, 202301 (2022).
- [27] J. Adam *et al.* (STAR Collaboration), Measurement of the mass difference and the binding energy of the hypertriton and antihypertriton, *Nat. Phys.* **16**, 409 (2020).
- [28] B. E. Aboona *et al.* (STAR Collaboration), Observation of directed flow of hypernuclei ${}^3_{\Lambda}\text{H}$ and ${}^4_{\Lambda}\text{H}$ in $\sqrt{s_{NN}} = 3\text{GeV Au} + \text{Au}$ collisions at RHIC, *Phys. Rev. Lett.* **130**, 212301 (2023).
- [29] NICA White Paper, <http://theor.jinr.ru/twiki/cgi/view/NICA/WebHome>.
- [30] J. Yang, J. W. Xia, G. Q. Xiao, H. S. Xu, H. W. Zhao, X. H. Zhou, X. W. Ma, Y. He, L. Z. Ma, D. Q. Gao *et al.*, High intensity heavy ion accelerator facility (HIAF) in China, *Nucl. Instrum. Methods Phys. Res. Sect. B* **317**, 263 (2013).
- [31] D. Gerstung, N. Kaiser, and W. Weise, Hyperon-nucleon three-body forces and strangeness in neutron stars, *Eur. Phys. J. A* **56**, 175 (2020).
- [32] D. Lonardonì, A. Lovato, S. Gandolfi, and F. Pederiva, Hyperon puzzle: Hints from quantum Monte Carlo calculations, *Phys. Rev. Lett.* **114**, 092301 (2015).
- [33] Z. Q. Feng, Formation and dynamics of exotic hypernuclei in heavy-ion collisions, *Phys. Rev. C* **102**, 044604 (2020).
- [34] C. Rappold, T. R. Saito, O. Bertini, S. Bianchin, V. Bozkurt, E. Kim, M. Kavatsyuk, Y. Ma, F. Maas, S. Minami *et al.*, Hypernuclear production cross section in the reaction of ${}^6\text{Li} + {}^{12}\text{C}$ at 2A GeV, *Phys. Lett. B* **747**, 129 (2015).
- [35] A. Le Fèvre, J. Aichelin, C. Hartnack, and Y. Leifels, FRIGA: A new approach to identify isotopes and hypernuclei in n -body transport models, *Phys. Rev. C* **100**, 034904 (2019).
- [36] H. G. Cheng and Z. Q. Feng, Hyperon dynamics and production of multi-strangeness hypernuclei in heavy-ion collisions at 3A GeV, *Phys. Lett. B* **824**, 136849 (2022).
- [37] STAR Collaboration, Production of protons and light nuclei in Au + Au Collisions at $\sqrt{s_{NN}} = 3\text{ GeV}$ with the STAR detector, [arXiv:2311.11020](https://arxiv.org/abs/2311.11020).
- [38] A. S. Botvina, K. K. Gudima, and J. Pochodzalla, Production of hypernuclei in peripheral relativistic ion collisions, *Phys. Rev. C* **88**, 054605 (2013).
- [39] A. S. Botvina, K. K. Gudima, and J. Steinheimer, Formation of hypernuclei in heavy-ion collisions around the threshold energies, *Phys. Rev. C* **95**, 014902 (2017).
- [40] A. S. Botvina, K. K. Gudima, J. Steinheimer, M. Bleicher, and I. N. Mishustin, Production of spectator hypermatter in relativistic heavy-ion collisions, *Phys. Rev. C* **84**, 064904 (2011).
- [41] A. Ono, Cluster correlations in multifragmentation, *J. Phys.: Conf. Ser.* **420**, 012103 (2013).
- [42] A. Ono, Cluster production within antisymmetrized molecular dynamics, *EPJ Web Conf.* **122**, 11001 (2016).
- [43] R. Wang, Y. G. Ma, L. W. Chen, C. M. Ko, K. J. Sun, and Z. Zhang, Kinetic approach of light-nuclei production in intermediate-energy heavy-ion collisions, *Phys. Rev. C* **108**, L031601 (2023).
- [44] C. Kuhrtz, M. Beyer, P. Danielewicz, and G. Röpke, Medium corrections in the formation of light charged particles in heavy ion reactions, *Phys. Rev. C* **63**, 034605 (2001).
- [45] P. Danielewicz and G. F. Bertsch, Production of deuterons and pions in a transport model of energetic heavy-ion reactions, *Nucl. Phys. A* **533**, 712 (1991).
- [46] P. Danielewicz and Q. Pan, Blast of light fragments from central heavy-ion collisions, *Phys. Rev. C* **46**, 2002 (1992).
- [47] G. Röpke and H. Schulz, Including cluster formation into a Vlasov-Uehling-Uhlenbeck approach to intermediate energy heavy ion collisions, *Nucl. Phys. A* **477**, 472 (1988).
- [48] D. Oliinychenko, L-G Pang, H. Elfner, and Volker Koch, Microscopic study of deuteron production in PbPb collisions at $\sqrt{s} = 2.76\text{ TeV}$ via hydrodynamics and a hadronic afterburner, *Phys. Rev. C* **99**, 044907 (2019).
- [49] J. Staudenmaier, D. Oliinychenko, J. M. Torres-Rincon, and H. Elfner, Deuteron production in relativistic heavy ion collisions via stochastic multiparticle reactions, *Phys. Rev. C* **104**, 034908 (2021).
- [50] K. J. Sun, R. Wang, C. M. Ko, Y. G. Ma, and C. Shen, Unveiling the dynamics of nucleosynthesis in relativistic heavy-ion collisions, [arXiv:2207.12532](https://arxiv.org/abs/2207.12532).
- [51] C. Frosin *et al.* (INDRA-FAZIA Collaboration), Examination of cluster production in excited light systems at Fermi energies from new experimental data and comparison with transport model calculations, *Phys. Rev. C* **107**, 044614 (2023).
- [52] G. Tian, Z. Chen, R. Han *et al.*, Cluster correlation and fragment emission in ${}^{12}\text{C} + {}^{12}\text{C}$ at 95 MeV/nucleon, *Phys. Rev. C* **97**, 034610 (2018).
- [53] G. Coci, S. Glassel, V. Kireyeu, J. Aichelin, C. Blume, E. Bratkovskaya, V. Kolesnikov, and V. Voronyuk, Dynamical mechanisms for deuteron production at mid-rapidity in relativistic heavy-ion collisions from SIS to RHIC energies, *Phys. Rev. C* **108**, 014902 (2023).
- [54] J. Aichelin, “Quantum” molecular dynamics—a dynamical microscopic n -body approach to investigate fragment formation and the nuclear equation of state in heavy ion collisions, *Phys. Rep.* **202**, 233 (1991).
- [55] S. Hudan *et al.*, Characteristics of the fragments produced in central collisions of ${}^{129}\text{Xe} + \text{nat Sn}$ from 32A to 50A MeV, *Phys. Rev. C* **67**, 064613 (2003).
- [56] K. Zbiri *et al.*, Transition from participant to spectator fragmentation in Au + Au reactions between 60A and 150A MeV, *Phys. Rev. C* **75**, 034612 (2007).
- [57] W. Reisdorf *et al.*, Systematics of central heavy-ion collisions in the 1A GeV regime, *Nucl. Phys. A* **848**, 366 (2010).
- [58] C. Xu, Z. Ren, G. Röpke, P. Schuck, Y. Funaki, H. Horiuchi, A. Tohsaki, T. Yamada, and B. Zhou, α -decay width of ${}^{212}\text{Po}$ from a quartetting wave function approach, *Phys. Rev. C* **93**, 011306(R) (2016).
- [59] Z. Q. Feng, Momentum dependence of the symmetry potential and its influence on nuclear reactions, *Phys. Rev. C* **84**, 024610 (2011).
- [60] T. Maruyama, K. Niita, and A. Iwamoto, Extension of quantum molecular dynamics and its application to heavy-ion collisions, *Phys. Rev. C* **53**, 297 (1996).
- [61] Akira Ono, Online talk with the title of cluster production in expanding nuclear matter in intermediate-energy heavy-ion collisions, <https://www.youtube.com/watch?v=idZMEu4IBXw>.
- [62] D. H. Boal and J. N. Glosli, Quasiparticle model for nuclear dynamics studies: Ground-state properties, *Phys. Rev. C* **38**, 1870 (1988).
- [63] G. Peilert, J. Randrup, H. Stöcker, and W. Greiner, Clustering in nuclear matter at subsaturation densities, *Phys. Lett. B* **260**, 271 (1991).

- [64] G. Peilert, J. Konopka, H. Stöcker, and W. Greiner, Dynamical treatment of Fermi motion in a microscopic description of heavy ion collisions, *Phys. Rev. C* **46**, 1457 (1992).
- [65] M. Papa, T. Maruyama, and A. Bonasera, Constrained molecular dynamics approach to fermionic systems, *Phys. Rev. C* **64**, 024612 (2001).
- [66] Y. Kanada-En'yo, H. Horiuchi, and A. Ono, Structure of Li and Be isotopes studied with antisymmetrized molecular dynamics, *Phys. Rev. C* **52**, 628 (1995).
- [67] K. Hagel *et al.*, Violent collisions and multifragment final states in the $^{40}\text{Ca} + ^{40}\text{Ca}$ reaction at 35 MeV/nucleon, *Phys. Rev. C* **50**, 2017 (1994).